A Flow Model for the Settling Velocities of non Spherical Particles in Creeping Motion

Y. Mendez†

Faculty of Engineering, Carleton University, Ottawa, Ontario, K1S 5B6

†*Corresponding Author Email: ymzarate@connect.carleton.ca*

ABSTRACT

This paper undertakes a critical examination of Stokes' law in its final form. The examination and insights of the viscosity principle substantiate grounds to suspect that the controlling dynamics are viscous shear rates across a geometry set by solid boundaries only. The examination sets grounds to conduct an analysis of the dynamics based on the viscosity principle alone and a flow model is derived. Based on the relationship between the pressure gradient and the shear forces as mandated by the viscosity principle the analysis suggests that the pressure gradient surrounding settling particles can be computed, is a single value and expands as required to mobilize a force equal to the driving force. In this context, the pressure gradient arises as a consequence of the contest between body forces in the fluid and the shear forces promoted by shear rates. The flow model suggests that Stokes' law may be missing important information. An analysis is conducted for the settling velocity of non spherical particles based on the same dynamics and a mathematical solution is reached. The solution is in good agreement with published measured values and defines the influence of particle shape in settling phenomena.

Keywords: Sedimentation, Tributary volume, Wall shear, Expansion, Stokes' law, Aspect ratio.

NOMENCLATURE

Ac	surface area of a coin like solid	h_{emax}	maximum non spherical expansion
Ao	surface area of a an oblate spheroid	h_g	height
ASS	specific surface area	h_{gmax}	maximum height
$ASSc$	specific surface area of a coin like solid	h_{max}	maximum tributary volume
$ASSo$	specific surface area of an oblate spheroid	P	Pressure
a	radius of an oblate spheroid	R	maximum radius of a spherical system
a_r	aspect ratio	r	radius
b	½ the thickness of an oblate spheroid	u	velocity
e	tributary ratio	V_f	volume enclosed between two concentric spheres
e_1	pseudo tributary ratio		
e_{1max}	maximum pseudo tributary ratio	V_{max}	maximum velocity
e_{max}	maximum tributary ratio	V_s	settling velocity
F_d	drag force	μ	viscosity
F_v	viscous drag force	μ_h	viscosity in the tributary volume
Gs	specific gravity of solid	σ	vertical stress
G_{sf}	specific gravity of fluid	ξ	spherical expansion
$f(a,b)$	function of a and b	ξ_{max}	maximum spherical expansion
g	acceleration due to gravity	τ	shear stress
h	tributary volume	τ_w	wall shear
h_e	non spherical expansion		

1. INTRODUCTION

Stokes' law and its applications are well known by the scientific and engineering community worldwide. Its derivation is readily available and its weaknesses and strengths have been highlighted widely in the literature.

Criticism of its final form for the settling velocities of spheres is rare since one, it correlates very well with experimental data and two, is rendered with the authority of being an analytical solution of a simplified

Navier Stokes equation.

Since the early 1900's scrutiny of the relationship has assumed Stokes' relationship as being a law at infinite dilution. The consensus has remained nearly flawless for more than a hundred years. Recently, Goodstein (2001) points out Millikan (1913) attempt to apply a correction procedure to Stokes' law and cast the qualifying statement "the nineteenth-century hydrodynamicist George Stokes had produced an exact formula applicable to a sphere moving slowly through an infinite, continuous viscous medium". Nevertheless, within a different trend of thought Jinghwa (2004), after 25 years of teaching experience recognizes with regard to Stokes' law "My students were totally confused. I myself did not quite understand the physics of the problem, even though I could follow Stokes' mathematical solution step by step" and continues in the next paragraph "In hydraulic engineering, Stokes' law is presented as an experimental relation, an empirical law, valid for a limited range of conditions". It is not the purpose of this examination to undertake a struggle through the dynamics of the mathematical formulation as the efforts of 25 years by Jinghwa Hsü and many other scientists have led to enlightening conclusions. The examination is intended to gather information and insights that could lead to a better understanding of creeping flow. The insights led to a fresh analysis of the problem and became the driving force behind this paper and presented below.

Let us examine the velocity between two plates driven by a pressure gradient in laminar flow with a coordinate system at midpoint between the plates and the *x* axis oriented horizontally positive with the pressure gradient:

$$u = \frac{dp}{dx} \frac{h^2}{2\mu} \left(1 - \frac{y^2}{h^2} \right) \tag{1}$$

Where:
u = the velocity at any point between the plates
$\frac{dp}{dx}$ = the pressure gradient in the x direction
h = ½ the distance between the two plates
μ = the viscosity
The maximum velocity V_{max} at $y = 0$ turns into

$$V_{\max} = \frac{dp}{dx} \frac{h^2}{2\mu} \tag{2}$$

As a consequence of the previous relationship and in virtue of the viscosity principle the shear stress τ at any point can be written as:

$$\tau = \frac{dp}{dx} y \tag{3}$$

At the wall $y = h$ and the shear stress $\tau = \tau_w$, hence:

$$\tau_w = \frac{dp}{dx} h \tag{4}$$

Note from Eq. (1) that for application of the viscosity principle the geometry is set externally and the shear stresses act along surfaces that are parallel to the shear surface at the boundaries; integration of the shear stresses along surfaces of defined geometry lead to the velocity. The simple relationship in Eq. (2) for the maximum velocity is just a single value on the curve. Note also that the pressure gradient is constant at any point and the shear stress at any surface is the product of the pressure gradient times the tributary volume of fluid overlying that surface. An interesting fact is that the pressure gradient act in the volume, thus, what has been quoted as a "height" or ½ the distance between the two plates is a tributary volume (m^3/m^2) over the square meter of surface. Technically, the drag force of the creeping motion is simply the wall shear τ_w times the area of the plate, no pressure drag is present, neither necessary. Moreover, one can categorically state, in laminar creeping motion, that a relationship of the form pressure gradient times "height" squared divided by the viscosity will give the velocity at some point in a profile of fluid.

2. STOKES' LAW

Stokes' relationship for the settling velocity *Vs* in creeping flow is presented below:

$$V_s = \frac{2(\rho_s - \rho_f) g r^2}{9\mu} \tag{5}$$

where:

ρ_s = the density of the solid
ρ_f = the density of the fluid
g = the gravitational constant
r = the radius of a settling sphere of density ρ_s.
Reordering Stokes' law we obtain:

$$V_s = \frac{4(\rho_s - \rho_f) g}{9} \frac{r^2}{2\mu} \tag{6}$$

The fraction on the right side makes up a pressure gradient; times "height" squared equal the velocity at some point in a profile. Stokes' analytical solution seem to have concluded that the settling velocity of a particle is the same as the maximum velocity (or fraction thereof) between two flat plates at distance *2r* driven by a pressure gradient *4(ρs-ρw)g/9*. Note that it can only be shear stresses integrated along a planar surface as there is no other geometry factors to make a "statement" of the spherical nature of the surfaces, if it is that the viscosity principle is to be satisfied and integration across geometry, set by the solid surface is possible. However, examination of its form and its success provide substantial evidence that in creeping flow the viscous shear is the controlling operator, there is nothing available in the relationship to link to the kinetic energy or pressure drag. To emphasize the dependence of the motion to shear rates across a velocity profile, let us examine Stokes' law for the drag force F_d mobilized by a particle settling at velocity *Vs* presented below:

$$F_d = 6\pi r \mu V_s \tag{7}$$

In arriving to the previous relationship the analytical solution claims to have encountered the form of a vertical stress σ acting on the entire surface presented below:

$$\sigma = \frac{3\mu V_s}{2r} \qquad (8)$$

Consequently, Eq. (7) is obtained by multiplying the stress by the area. The dynamics of the forces that convert tangential shear forces at any angle to a single value of stress acting vertically at any point cannot be explained. Note however that according to the viscosity principle and the relationship between the shear stresses and the pressure gradient the shear stress at the wall can be written as:

$$\tau_w = \frac{dp}{dx} h = \frac{2\mu V_{\max}}{h} \qquad (9)$$

In form, identical to Stokes "complex" vector quantity. As mentioned previously for a laminar viscous regime the drag force F_v is simply the wall shear times the area. Let us assume $h = r$ and apply the force to the entire area of a sphere:

$$F_v = \frac{2\mu V_{\max}}{r} 4\pi r^2 = 8\pi r \mu V_{\max} \qquad (10)$$

a conclusion almost identical to that delivered by the analytical solution in the absence of consideration of any pressure drags. As far as the logic of the principles set by the viscosity, Stokes' law is the value of shear stress at some point across a flat profile between two plates at distance *2r* multiplied by the area. This drag force depends on the viscosity alone. A fact that emphasizes viscous shear rates across the geometry set by solid boundaries as the controlling dynamics.

The previous insights made a strong case for a re-examination of the problem based on the viscosity principle alone. The examination led to the analysis presented below.

3.   FORCE TRANSFER

Consider a settling sphere. At the beginning of the settling process the solid body simultaneously forces the fluid outward in a radial direction and sucks at the top pole causing a resultant tangential force. The tangential force finds opposition to the movement by shear forces in the fluid; the Newtonian condition mandates a shear response equal to zero at the beginning and acquires a value as soon as the motion starts and the viscosity principle govern the motion as the driving forces are comparable with shear stress mobilized by the fluid. Shear rates are originated in this process and extend outward at decreasing shear rates as much as necessary to mobilize across the volume a force equal to the skin force. According to the definitions set by the viscosity principle the contest between the shear forces and the body forces become a pressure gradient and the equilibrium condition is set by a transfer of force equal to the gravitational force. The particle forms a system that makes his way downward by displacing fluid by shear rates. As noted in the treat to highlights of the viscosity principle the value of the shear stress at any point throughout the profile is defined by a single value of pressure gradient acting on the fluid overlying any given spherical surface. Any imbalance in the ambient pressure gradient yield to an equilibrium value. According to the previous scheme

the inter phase between the solid and the fluid continuum offer the single available mean to transfer the submerged weight, a known quantity, by means of shear rates to the fluid. This fact imposes the first question, how would the solid phase transfer its energy through the skin?. Consider an object of area *A* and mass *M*; by definition in the absence of buoyancy the specific surface area *ASS* (in units of m2/kg for this discussion) is *A/M*, hence the quantity $ASS^{-1}g$ (N/m2), the inverse of the specific surface area, times the gravitational constant expresses the gravitational force available to be transferred in the form of shear stress to a viscous medium or the wall shear of the particle. The submerged weight *Ws* of a solid of weight *W* and specific gravity G_s within a fluid of specific gravity G_{sf} can be shown to be *Ws =((Gs - Gsf)/ Gs)W*; hence, the wall shear τ_w of the submerged particle can be written as:

$$\tau_w = \frac{1}{ASS} \frac{\left(G_s - G_{sf}\right)}{G_s} g \qquad (11)$$

Note that the solid continuum is bounded to the skin, the only available mean to transfer the force to the fluid continuum and that the dynamics of the motion mandate a single value response by the fluid on the skin or wall, hence, the previous parameter appear to be an ideal measure of the driving force. The wall shear times the area of the particle equal to the submerged weight of the particle. Let us conduct an enquiry on whether the portrayed dynamics can realistically be linked to the settling phenomena or not with measured settling velocities for quartz sand (*Gs = 2.65*) in water at *15 Cᵒ* (*ρf = 999* kg/m3 and *μ = 0.001139* Pa-s) from Zegzhda (1934), Arkangel'skii (1935) and Sarkisyan (1958) reproduced by Cheng (1997) shown in Table 1. It is found that *Vs* is proportional to τ_w^2 in the form *Vs ≈ 0.0775 τ_w^2*. Note also that for a particle of sand with G_s = 2.65 in water the wall shear take the value of *0.0027 N/m²*, a value comparable with the viscosity itself and by the definition $\mu(du/dy) = \tau$ the shear rate at the wall can be computed as τ_w/μ. For a sphere of density ρ_s, *ASS* takes the form *ASS = 3/(rρ_s)* and Eq. (11) turns into:

$$\tau_w = \frac{r\rho_s}{3} \frac{\left(G_s - G_{sf}\right)}{G_s} g \qquad (12)$$

The possibility of relating the specific surface area to a characteristic dimension for spheres makes an advantage for the application of the viscosity principle as the driving force grows at the same pace as the characteristic dimension for different particle sizes. For other geometries commonly encountered in geological materials this advantage is not available. This is suspected to be the reason of the difficulty of applying Stokes' law to different geometries.

4.   GEOMETRY

Establishing the geometrical settings and the physical dimensions of the system has been shown to be the most relevant condition in order to quantify shear forces based on the viscosity principle. Integration through the geometry or "height" delivers the velocity. Consider a point symmetric spherical system; the velocity and shear stress is maximum at the solid surface and zero at

some point, the pressure gradient yield to an equilibrium value, is ambient and depends on the contest between the shear stresses and body forces on the mass of the fluid, the driving force is shear rate at the wall. Consider a sphere of radius R enclosing the velocity profile and defining the size of the entire system (including fluid and solids) at the point of zero shear stress and a smaller sphere of radius r within the fluid at the same center point (not necessarily the solid sphere of radius r_s). The volume of fluid V_f between the two spheres can be computed as:

$$V_f = \frac{4}{3}\pi R^3 - \frac{4}{3}\pi r^3 \qquad (13)$$

And the ratio e of the volume V_f to the volume of the smaller sphere can be computed as:

$$e = \frac{\frac{4}{3}\pi R^3 - \frac{4}{3}\pi r^3}{\frac{4}{3}\pi r^3} = \frac{R^3 - r^3}{r^3} \qquad (14)$$

denoted e to take advantage of the void ratio, a widely known parameter in geotechnical engineering that is defined similarly. The tributary ratio will be term used in this paper. The maximum tributary ratio e_{max} can be computed at the wall of the solid, where $r = r_s$ as:

$$e_{max} = \frac{\frac{4}{3}\pi R^3 - \frac{4}{3}\pi r_s^3}{\frac{4}{3}\pi r_s^3} = \frac{R^3 - r_s^3}{r_s^3} \qquad (15)$$

According to the previous definition of e the following relationship is satisfied $(4/3)\pi r_s^3(1+e) = (4/3)\pi R^3$; R can be written as:

$$R = r_s(1+e)^{\frac{1}{3}} \qquad (16)$$

At the wall $r = r_s$, $e = e_{max}$ and R can be computed as:

$$R = r_s(1+e_{max})^{\frac{1}{3}} \qquad (17)$$

The height or distance h_g (the subscript g to denote geometric height) measured from R of the overlying fluid on any square meter of the sphere of radius r can be calculated as $h_g = R-r$; hence:

$$h_g = r_s\left(\left(\sqrt[3]{1+e}\right)-1\right) \qquad (18)$$

The maximum distance h_{gmax} occurs at the wall with $r = r_s$ and $e = e_{max}$, hence:

$$h_{g\,max} = r_s\left(\left(\sqrt[3]{1+e_{max}}\right)-1\right) \qquad (19)$$

The tributary volume h in m³/m² of the fluid V_f overlying the area of the sphere of radius r can be expressed in the form:

$$h = \frac{\frac{4}{3}\pi R^3 - \frac{4}{3}\pi r^3}{4\pi r^2} = \frac{R^3 - r^3}{3r^2} \qquad (20)$$

The tributary volume takes its maximum value h_{max} at the wall with $r = r_s$, and $e = e_{max}$ hence:

$$h_{max} = \frac{r_s^3(1+e_{max})-r_s^3}{3r_s^2} = \frac{e_{max}\,r_s}{3} \qquad (21)$$

Equations (18) and (20) show that for a spherical system h_g and h are different as oppose to a planar flow in which h_g and h are the same and there is no need to define them separately. It also shows that application of the viscosity principle in a loose boundary requires due consideration to the volumetric nature of the pressure gradient. Ignoring this fact induce a violation of the dynamics by the breakdown of the constituent relationship between the pressure gradient and the shear rates. The computed values would hence deviate from experimental values. The viscosity is an operator in the geometry domain or the height h_g but the pressure gradient bears a volumetric relationship with the shear stress at any point through the profile.

Equation (20) quantify the dimensions of the volume domain and how it relates in the per meter square basis to the entire size of the system and provide an appropriate mean to conduct the integration to obtain the velocity. In other words in a spherical system of radius R Eq. (20) allows for the computation of the tributary volume overlying any spherical surface of radius r.

Noting that $3/r_s = \rho_s\,ASS$ the maximum tributary volume can also be expressed as:

$$h_{max} = \frac{e_{max}}{\rho_s\,ASS} \qquad (22)$$

5. THE WALL SHEAR AND THE SETTLING VELOCITIES

Consider a spherical coordinate system attached to the center of a settling sphere with wall shear τ_w and a horizontal plane across the center. Consider the geometric settings envisioned in the previous section, and the dynamics of the force transfer. A ring of influence of the viscous shear is formed and the surrounding fluid is static. Any streamline is contained on a vertical plane through the center of the sphere, is parallel to the surface of the solid sphere and an identical velocity profile forms perpendicular to any line crossing the center of the sphere; the flow is fully developed and spherical. Equation (20) solves for the quantification of the dimensions of shear surfaces as they relate to the entire system and sets grounds for integration across the geometry preserving the volumetric relationship between the pressure gradient and the shear stresses. The pressure gradient at any distance r within the profile $p(r)$ is identical at any point and by definition can be expressed as $p(r) = \tau_w/h_{max}$; the shear stress at any point across the profile is related to the pressure gradient and the tributary volume h in m³/m² by the relationship $\tau = p(r)h$, where h is measured from the point of zero shear stress and given that the velocity u, the viscosity μ and the shear stress τ are related by $\tau = \mu(du/dr)$ one can write:

$$\mu\frac{du}{dr} = -\tau_w\,\frac{h}{h_{max}} \qquad (23)$$

In consideration that the geometry of the profile is identical at any location and the tributary volume h at any distance r from the center of the spherical coordinate system with respect to a boundary surface at a distance R defined by zero shear stress can be expressed from Eq. (20) as:

$$h = \frac{r^3 - R^3}{3r^2} \qquad (24)$$

Equation (23) takes the form:

$$\mu \frac{du}{dr} = \frac{-\tau_w}{h_{max}} \frac{\left(r^3 - R^3\right)}{3r^2} \qquad (25)$$

Equation (25) paves the way to conduct the integration across the geometry of the profile and maintain the integrity of the relationship between the tributary volume and the shear stresses. Solving for the velocity, Eq. (25) takes the form:

$$u = \frac{-\tau_w}{2\mu h_{max}} \frac{\left(2R^3 + r^3\right)}{3r} + C \qquad (26)$$

At $r=R$, $u = 0$; hence $C = \dfrac{\tau_w R^2}{2h_{max}\mu}$, which leads to:

$$u = \frac{-\tau_w}{2\mu h_{max}} \left(\frac{r^2}{3} + \frac{2R^3}{3r} - R^2 \right) \qquad (27)$$

substituting r in virtue of Eq. (18) to write as a function of the tributary ratio we obtain:

$$u = \frac{-3\tau_w}{2\mu e_{max} r_s} \times$$
$$\left(\frac{r_s^2 (1+e)^{\frac{2}{3}}}{3} + \frac{2(1+e_{max})r_s^3}{3r_s(1+e)^{\frac{1}{3}}} - (1+e_{max})^{\frac{2}{3}} r_s^2 \right) \qquad (28)$$

The maximum velocity V_{max} occurs where $r = r_s$ and the tributary ratio e equal zero, hence:

$$V_{max} = \frac{-3\tau_w r_s}{2\mu} \left(\frac{1}{e_{max}} + \frac{2}{3} - \frac{(1+e_{max})^{\frac{2}{3}}}{e_{max}} \right) \qquad (29)$$

Our treat shows that the maximum velocity and shear stress occurs at the wall, hence, $V_{max} = V_s$. The wall shear is available and matching to the experimental settling velocity results for quartz sand particles 0.5 to 25.0 μm in water at 15 C^o shown in Table 1. (G_s taken as 2.65, $\mu = 0.001139$ $Pa\text{-}s$ and $\rho_f = 999.3$ Kg/m^3) from Zegzhda (1934), Arkangel'skii (1935) and Sarkisyan (1958) reproduced by Cheng (1997), we find the tributary ratio $e_{max} = 16.34$ from Eq. 29. Equation 28 reaches a great accomplishment by allowing the settling velocity to be written entirely as a function of e_{max} with all other known values. Note also that the viscosity principle dictates that the ratio of the shear stress at any given surface divided by the tributary volume overlying that surface equals the pressure gradient in the form $\tau = p(r)h$. At the wall the values can be computed as:

$$\tau_w / h_{max} = P(r) \qquad (30)$$

Substituting the wall shear and the maximum tributary volume from Eqs. (11) and (21) respectively, we obtain:

$$P(r) = \frac{\dfrac{r\rho_s}{3} \dfrac{\left(G_s - G_{sf}\right)}{G_s} g}{\dfrac{e_{max} r}{3}} = \frac{\left(G_s - G_{sf}\right)}{e_{max} G_s} g\rho_s \qquad (31)$$

The tributary volume and the wall shear increase with the radius of the particle and the pressure gradient is constant at *991N/*m^3 for the given value of density and viscosity of the fluid at standard temperature of 15 ^{o}C. Equation (31) implies that the pressure gradient times the volume held within the limits of the ambient pressure gradient equal the submerged weight of the particle as verified for the sand particle of 0.5 μm radius $F = (4/3)\pi r_s^3 e_{max} P(r) = 8.48 \times 10^{-15}N$. The equilibrium condition is set by the transfer of a force equal to the submerged weight of the particle to the fluid medium in the form of a pressure gradient. The same conclusion is reached by noting that for a sand particle *0.5 μm* the wall shear can be computed from Eq. (12), $\tau_w = 0.0027$ *N/m^2* and the tributary volume $h_{max} = e_{max}r/3 = 2.723 \times 10^{-6}m$, hence, $P(r) = 991$ N/m^3.

For convenience, based on our acquired knowledge let us rewrite Eq. (27) substituting the pressure gradient from Eq. (30) as:

$$u = \frac{-P(r)}{2\mu} \left(\frac{r^2}{3} + \frac{2R^3}{3r} - R^2 \right) \qquad (32)$$

consequently Eq. (28) can be written as:

$$u = \frac{-P(r)}{2\mu} \times$$
$$\left(\frac{r_s^2 (1+e)^{\frac{2}{3}}}{3} + \frac{2(1+e_{max})r_s^3}{3r_s(1+e)^{\frac{1}{3}}} - (1+e_{max})^{\frac{2}{3}} r_s^2 \right) \qquad (33)$$

Equation (33) is equivalent to Eq. (32) as a function of e and the value of the velocity can be computed for the entire velocity profile by varying e from *0* to e_{max} to compute the radius and apply the relationship. For the maximum velocity at the wall of the particle (or $e = 0$) the settling velocity is computed as:

$$V_s = \frac{-P(r)r_s^2}{2\mu} \left(1 + \frac{2e_{max}}{3} - (1+e_{max})^{\frac{2}{3}} \right) \qquad (34)$$

In further discussion the relationship between brackets in Eq. (33) will be quoted as the spherical expansion ζ and the maximum spherical expansion ζ_{max} from the large brackets in Eq. (34) is constant at the given value of density and viscosity of the fluid for the given specific gravity of solids. Table 1 presents comparison of settling velocities computed from Eq. (29) and the experimental values for sand particles 0.5 to 25.0 μm (Gs taken as 2.65) from Zegzhda (1934), Arkangel'skii (1935) and Sarkisyan (1958) reproduced by Cheng (1997). Note in Table 1 that V_s is computed using Eq. (29) but the same result is accomplished by Eq. (34). The velocity profile from Eq. (32) for the particle $r_s = 0.5$ μm is shown in Fig. 1. Note in Fig. 1 that the geometry is defined by the pressure gradient,

the velocity is cero at $r = R = 1.29\ \mu m$ (or $e = e_{max}$) and maximum at the wall of the solid sphere ($r = r_s$ or $e = 0$). The conclusion drawn in Eq. (31) shows that the specific gravity has no impact in the pressure gradient; instead, the different specific gravities change the size of the expansion. For instance a particle *A* of specific gravity 2.8 has a maximum tributary ratio 17.8 (Eq. (31)) and a maximum expansion $\xi_{max} = 5.8$ and a particle *B* of $G_s = 2.4$ has a maximum tributary ratio of 13.85 and the maximum expansion $\xi_{max} = 4.19$. Particle *A* settles 38% faster with respect to *B*. This result is in contrast with a difference of 29% predicted by Stokes.

Table 1 Calculated settling velocities from Eq. (29) and experimental values for sand in water at *15 C^o from* Zegzhda (1934), Arkangel'skii (1935) and Sarkisyan (1958) reproduced by Cheng, N. (1997). Average error less than 1%.

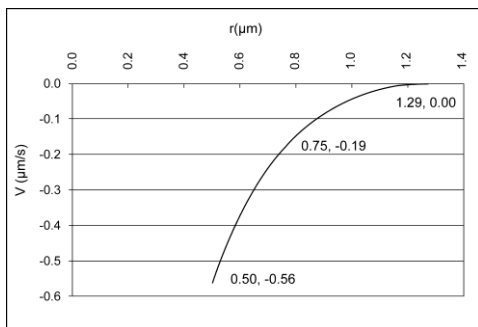| r (μm)	Computed from Eq. 12 $Tw\ (mPa)$	Computed from Eq. 29 $Vs\ (\mu m/s)$	Measured $(\mu m/s)$
0.5	2.70	0.56	0.57
2.5	13.49	14.11	14.10
5.0	26.97	56.46	56.50
10.0	53.94	225.83	223.00
25.0	134.85	1411.42	1410.00

Fig. 1. Velocity profile for a 0.5 μm sand particle in water at 15° C

6. NON SPHERICAL GEOMETRIES

In terms of science and engineering the greater interest for a flow model for the settling velocity of non spherical geometries is by far on its applicability to natural occurring materials such as clay minerals. In sedimentation analysis the selection of a geometry model for clay particles is often necessary. The general intend of this section is to emphasize the need to select a geometry model describing as closely as possible the volume-mass-area relationships of the particles. In general, morphology treats describe clay particles in terms of mean dimensions: thickness, lengths, slenderness and specific surface area. Thicknesses and specific surface areas are somewhat stable quantities for different minerals. It doesn't seem feasible to work with *ASS* only as the viscosity is an operator in the geometry of the ambient fluid. For non spherical geometries, the need arises to describe the particle in at least 2 dimensions. Clay particles are widely described in the literature as platelets of oblate spheroid geometry. For

instance, Sayed *et al.* (2006) based on atomic force microscopy (AFM) display how particles are sliced in planes perpendicular to the minor axis to estimate edge and basal areas. The edge of the planes appear as concentric circles that further support the oblate spheroid shape. The procedure used by Sayed *et al.* (2006) is supported by previous research starting with Bickmore *et al.* (2002) and Jodin *et al.* (2004). Within a similar trend they are often described as coins with the measured basal areas and thicknesses. Based on morphology treats it appears feasible to describe a wide variety of clay particles in two dimensions. The specific surface area of oblate spheroids *ASSo* and coins *ASSc* of density ρ_s and dimensions ½ the length and ½ the thickness *a* and *b* respectively is presented below:

$$ASSo = \frac{2\pi a^2 \left(1 + f(a,b)\right)}{\frac{4}{3}\pi a^2 b \rho_s} = \frac{3\left(1 + f(a,b)\right)}{2b\rho_s} \tag{35}$$

$$ASSc = \frac{a + 2b}{ab\rho_s} \tag{36}$$

The term between brackets in Eq. (35) is a complex term. For aspect ratio $a_r = 8$ Eqs. (35) and (36) turn into:

$$ASSo = \frac{3(1.044)}{2b\rho_s} \tag{37}$$

$$ASSc = \frac{5}{4b\rho_s} \tag{38}$$

respectively. The difference is 25 %. For aspect ratios up to 100 commonly reported in the literature for a number of clay minerals the difference can be verified to be 50 %. By means of Eq. (37) and Eq. (38) one can verify which model is better suited for the given mineral when specific surface areas are available. The oblate spheroid model often yields better match between the measured ASS and the reported morphology but the coin model appears feasible for some clay minerals where "distinct right angles" and uniform thickness have been observed such as those reported by Żbik and Smart (1998) for Georgia kaolinite (KGa-1). A hexagonal prism could also be used for KGa-1. Note in addition that the specific surface, for aspect ratios greater than 6, becomes insensitive to *a* i.e. for a given mineral thickness and a_r say 10 as reference value, an increase in a_r to 20, decreases the term $(1+f(a,b))$ from 1.030 to 1.009. The differences become smaller for higher aspect ratios and the specific surface area becomes virtually independent of *a* for a wide variety of clay minerals. The geometric issue is similar to that resulting by cutting a corner of a sheet of paper and calculate the specific surface area for the corner and the entire sheet; the values are virtually the same as the edge area does not significantly contribute to the area. Further examination confirm that the term $(1+f(a,b))$ can be simplified as:

$$1 + f(a,b) = 1 + \left(\frac{b}{a}\right)^{\frac{3}{2}} \tag{39}$$

The computed values from Eq. (39) for aspect ratios 4 to 20 vary less than 1% with respect to the exact formula. The term $(b/a)^{3/2}$ can be safely assumed to be 0

for $a_r > 20$. The area *Ao* of the oblate spheroid is suggested to be computed as:

$$Ao = 2\pi a^2 \left(1 + \left(\frac{b}{a} \right)^{3/2} \right) \tag{40}$$

The small differences in the specific surface area for aspect ratios greater than 6 allow for great advantage in characterizing the geometry of clay particles based on the specific surface area and rough knowledge of the aspect ratios to provide good estimates of the thickness by means of Eq. (35).

7. ANALYSIS

As a part of these undertaking, a solution for the settling velocity of non spherical particles was sought by characterizing the tributary volume in the geometry domain of non spherical geometries; an approach that is a prerequisite to apply the viscosity principle. Oblate spheroid geometry was used with the intent to identify a characteristic length that would correlate with the size and geometric height h_g as identified for spherical systems without altering the volumetric relationships. As previously envisioned, with the previous approach, a solution without adding unnecessary complexity was found to be very difficult. The reason for the difficulty is that the sought outcome is just as ambitious as to derive a characteristic dimension that allows for the computation of the entire set of volume mass area relationships for non spherical geometries. It is later found that the entire system can be better characterized in the tributary volume domain without compromising rational arguments, dynamics and precision. The latter findings are discussed below.

From the basis of the analyses conducted in this paper the following issues can be considered factual aspects of the geometric relationships between the fluid medium and the solids:

(1) The wall shear is constant through the entire surface of the particle. Hence, the tributary volume, by the definition $\tau_w/h_v = P(r)$, is constant through the entire fluid interstice but it varies in geometry.

(2) Despite the differences in geometry of the tributary volume the flow regime at any point cannot be considered independent of some average condition dictated by the constant pressure gradient. This condition makes an *x,y* characterization technically feasible

(3) The characterization of the tributary volume can be done independently of a detailed characterization in the geometric height domain (this will be shown later on this paper).

(4) The viscosity is an operator in the geometry domain. This raises the difficulty of obtaining a characteristic length of the solid that correlates with the geometry of the fluid medium and the driving force at the same time.

Due to (3) if one sets grounds for an operator in the tributary volume domain without compromising the

operator in the geometry domain (as it is still the controlling operator) many difficulties imposed by (4) may become removed.

Let us recover additional information from Eq. (25) shown below:

$$\mu \frac{du}{dr} = \frac{-\tau_w}{h_{max}} \left(\frac{r^3 - R^3}{3r^2} \right) \tag{41}$$

Re-writing as a function of the tributary ratio we obtain:

$$\mu \frac{du}{dr} = -p(r) \left(\frac{\frac{4}{3}\pi r_s^3 \left((1+e) - (1+e_{max}) \right)}{4\pi r_s^2 (1+e)^{\frac{2}{3}}} \right) \tag{42}$$

Note that between brackets the volume and the area are the required parameters, which are known quantities. Eq. (42) shows that as long as we can define the volume and the area of the particle we can calculate the tributary volume without any geometric correlation between the solids and the fluid medium which confirms the statement in (3). Equation (42) can potentially remove some difficulties in (4) to address the issue of non spherical geometries; however, Eq. (42) still has a serious limitation, e g. a characteristic dimension *r* that correlates with both, the driving force and the geometry of the fluid is not available, hence, integration with respect to *r* is useless. Let us define μ_h as the shear stress per unit velocity gradient with respect to the tributary volume *h* to satisfy $\mu_h(du/dh) = \mu(du/dr)$ and rewrite Eq. (36) as:

$$\mu_h \frac{du}{dh} = -p(r) \left(\frac{r_s \left((1+e) - (1+e_{max}) \right)}{3(1+e)^{\frac{2}{3}}} \right) \tag{43}$$

μ_h is an unknown operator. Note that for two concentric volumes *A* and *B*; *B* considered an expansion of *A*, the definition of the quantity *h* and h_g for the volumes *A* and *B* (m^3/m^2) imply that the greater the expansion is *B* from *A* the greater is the difference between the tributary volume and the geometric "height", *h* and h_g respectively and approximate the same value the smaller the expansion is *B* from *A*. In contrast for planar surfaces as shown in the examination of the viscosity principle *h* and h_g are the same quantity and the shear stresses can be quantified as $P(r)y$ or $\mu(du/dy)$ as $h_g = y = h$ at any point leading to the equation:

$$\mu \frac{du}{dy} = P(r)y \tag{44}$$

and the integration delivers $u = P(r)y^2/(2\mu) + C$. Setting the boundary conditions for the planar flow between two plates Eq. (44) turns into Eq. (1). However, for particles *A* and *B* Eq. (44) is not satisfied. The tributary volume *h* and *y* differ from one another by a different amount through the entire profile and the velocity with respect to the tributary volume *du/dh* differ from the velocity with respect to the distance *du/dr* by a different amount at every point. However, the product $\mu_h du/dh$ must yield the same value as $\mu du/dr$ implying that μ_h can not be a constant value. This fact emphasizes that μ is still the controlling operator and we are just trying to

find a mean to move the same operator to the volume domain. Returning to Eq. (43), between brackets we have $m^3/m^2 = m$. Hence, integration over the tributary volume can only lead to:

$$u = -\frac{p(r)}{2\mu_h}\left(\frac{r_s\left((1+e)-(1+e_{\max})\right)}{3(1+e)^{\frac{2}{3}}}\right)^2 + C \tag{45}$$

At $e = e_{max}$ $u = 0$, hence $C = 0$. Rewriting:

$$u = -\frac{p(r)r_s^2}{2\mu_h}\left(\frac{\left((1+e)-(1+e_{\max})\right)}{3(1+e)^{\frac{2}{3}}}\right)^2 \tag{46}$$

Let us denote h_e, the non spherical expansion, as the relationship between brackets in Eq. (46) and rewrite it as:

$$u = -\frac{p(r)r_s^2}{2\mu_h}(h_e)^2 \tag{47}$$

Solving Eq. (46) for the maximum velocity at $e = 0$ we obtain:

$$V_{\max} = -\frac{p(r)r_s^2}{2\mu_h}\frac{e_{\max}^2}{9} \tag{48}$$

Let us define the maximum non spherical h_{emax} as $h_{emax} = (e_{max}/3)$ in Eq. (42) and rewrite it as:

$$u = -\frac{p(r)r_s^2}{2\mu_h}(h_{e\max})^2 \tag{49}$$

and let us bring forward the equation for the settling velocity of spherical particles as a function of e from Eq. (33):

$$u = \frac{-P(r)r_s^2}{2\mu} \times$$
$$\left(\frac{(1+e)^{\frac{2}{3}}}{3} + \frac{2(1+e_{\max})}{3(1+e)^{\frac{1}{3}}} - (1+e_{\max})^{\frac{2}{3}}\right) \tag{50}$$

Technically, for a sphere, we can either conduct integration through the tributary volume or through r, the geometry domain, to obtain the same result. Equating both relationships should yield relevant information and insights. Let us substitute the expansion ξ in Eq. (50) and present the result of the equality of Eqs. (46) and (50):

$$\frac{\mu_h}{\mu} = \frac{h_e^2}{\xi} \tag{51}$$

μ_h is not a constant, it varies along the entire profile or where the shear stresses are being taken. As e tend to e_{max}, μ_h tends to μ, meaning simply that the relationship between the tributary volume and the geometric height becomes similar to that of a flat surface in which h and h_g are the same; note that the ratio h_e^2/ξ tends to one as e tend to e_{max} but it becomes undefined as $e = 0$. Nevertheless, we can write with impunity:

$$\frac{\mu_h}{\mu} = \frac{0.0001+h_e^2}{0.0001+\xi} \tag{52}$$

Note also that the greater the tributary volume the more it differs from the geometric height; hence, the shear stress per unit velocity gradient with respect to the tributary volume becomes a greater quantity. This should not be taken as to suggest a viscosity that varies depending on the geometry of the settling particle; instead, is a geometric consequence of moving the same controlling operator to the volume domain. It is apparent that a small tributary volume being held by a large sphere is "flatter" than a large tributary volume being held by a small sphere. As a consequence, Eq. (52) offers a mean to decide on the shape of the velocity profile based on the geometry of the particle itself. The evolution of μ_h for a larger sphere can successfully portray the flatter tributary volume of the flatter particle. This is equivalent to consider the surface of a quasi flat particle as a portion of a sphere somewhere approaching infinite. Let us deposit the amount of water held by a non spherical particle of a and b dimensions over a sphere of radius a to obtain the pseudo tributary ratio e_1 over that sphere as follows:

$$e_1 = \frac{\frac{4}{3}\pi a^2 be}{\frac{4}{3}\pi a^3} \Rightarrow e_1 = \frac{be}{a} \tag{53}$$

And the maximum pseudo tributary volume e_{1max} takes the value:

$$e_{1\max} = \frac{be_{\max}}{a} \tag{54}$$

It is expected based on the rational provided previously that the tributary volume over the particle of radius a is flatter, as expected for the non spherical particle. Eq. (53) furnishes the capacity to make a statement of the flatness of the tributary volume based on the geometry of the particle itself. The shear stress per unit velocity gradient with respect to the tributary volume takes the value:

$$\mu_h = \frac{\mu\left(\dfrac{\left((1+e_1)-(1+e_{1\max})\right)}{3(1+e_1)^{\frac{2}{3}}}\right)^2}{\left(\dfrac{(1+e_1)^{\frac{2}{3}}}{3} + \dfrac{2(1+e_{1\max})}{3(1+e_1)^{\frac{1}{3}}} - (1+e_{1\max})^{\frac{2}{3}}\right)} \tag{55}$$

or simply written as:

$$\mu_h = \frac{\mu\left(0.0001+h_{e1}^2\right)}{\left(0.0001+\xi_1\right)} \tag{56}$$

As stated previously if we accomplish our goal on (4) of conducting integration over the tributary volume and derive an expression for the variation of the shear stress per unit velocity gradient with respect to the tributary volume we only need to be able to describe the volume and the area of the particle. Let us apply our morphology model (volume and area) in Eq. (46):

$$u = -\frac{p(r)}{2\mu_h}\left(\frac{\frac{4}{3}\pi a^2 b\left((1+e)-(1+e_{max})\right)}{2\pi a^2(1+f(a,b))(1+e)\frac{2}{3}}\right)^2 \Rightarrow$$

$$u = -\frac{p(r)}{\mu_h}\frac{2b^2}{9(1+f(a,b))^2}\left(\frac{(e-e_{max})}{(1+e)\frac{2}{3}}\right)^2 \qquad (57)$$

Substituting μ_h according to Eq. (52):

$$u = -\frac{p(r)}{\mu}\frac{2b^2}{9(1+f(a,b))^2}\left(\frac{(e-e_{max})}{(1+e)\frac{2}{3}}\right)^2 \times \qquad (58)$$

$$\frac{(0.0001+\xi_1)}{(0.0001+h_{e1}^2)}$$

Solving for the maximum velocity with $e = 0$ and $e_1 = 0$ we obtain:

$$V_s = -\frac{p(r)}{\mu}\frac{2b^2 e_{max}^2}{9(1+f(a,b))^2}\frac{(0.0001+\xi_{1max})}{(0.0001+h_{e1max}^2)} \qquad (59)$$

or

$$V_s = -\frac{p(r)}{\mu}\frac{2b^2 e_{max}^2}{9(1+f(a,b))^2} \times$$

$$\frac{\left(0.0001+\left(1+\frac{2e_{1max}}{3}-(1+e_{1max})\frac{2}{3}\right)\right)}{\left(0.0001+\frac{e_{1max}^2}{9}\right)} \qquad (60)$$

Equation (60) removes the difficulty induced by the absence of a characteristic dimension that correlates with the driving force and the geometry of the fluid medium at the same time. By means of the relationship between the largest brackets in Eq. (57) an appropriate quantification of the tributary volume is made and the integrity of its relationship with the pressure gradient is preserved. Finally, by establishing the variation of the shear stress per unit velocity gradient with respect to the tributary volume, not only Eq. (52) gives meaning to the original integration due in Eq. (43) but also allows for a mean to make a statement of the flatness of the tributary volume based on the morphology of the particle.

Although, simple, Eq. (60) is the result of an intense scrutiny of the relationships between the viscosity principle, the geometry of the particles and their impact to the geometry of the fluid medium. It doesn't seem to incur in any significant violation of the controlling dynamics and because of its form could be used for many geometries with appropriate considerations for the ratio h_{e1}^2/ξ_{1max}. Note that the relationship between the large brackets in Eq. (57) is the same as h_e and in consequence, for a sphere the ratio h_e^2/h_{e1}^2 cancel and $\xi_1 = \xi$ i.e. the mission of the expansion is the transfer of the volumetric domain to the geometry domain that allows the use for the single value of viscosity. Finally, note that the ratio $(0.0001+h_{e1}^2)/(0.0001+\xi_1)$ varies

from 1.00 to 1.63 and from 1.00 to 1.07 for Kaolinite and Montmorillonite respectively.

8. VALIDATION

Consider the results published by Lu *et al.* (2000) who measured settling velocities of *Georgia Kaolinite* and report highly non spherical geometry with the average major dimension within the range of one to three *μm.*. The mean particle taken as an oblate spheroid with *2a = 2 μm*, aspect ratio of *10* and *Gs = 2.65*. The average length as furnished by a "limited representative elemental volume" by Scaning Electron Microscopy (SEM) analysis and the aspect ratio and specific gravity are representative values for the given mineral. Additional measurements by Lu *et al.* (2000) include mica particles ("platy flakes") of relatively uniform thickness between No. 200 and No. 325 sieves (*75 μm* and *43 μm* respectively) and *Gs* ≈ 2.82. SEM images of the tested samples are also presented in the subject paper showing an approximate average thickness in the order of 7μm and elongated particles exceeding by far the nominal range. The minimum and greatest length can be taken as being 43 *μm* and 100 *μm* with mean particle size of *71 μm*. For the geometry model the particles are taken as coin like structures. Note that for the specific gravities used, the maximum tributary ratio *e_max* computed from Eq. (31) and the pressure gradient of *991 N/m³* takes the values of 17.25 and 18.01 for Georgia kaolinite and mica respectively. Another set of experimental values from settlement experiments to consider are those presented by Pruett and Webb (1993) and Żbik and Smart (1998). Pruett and Webb state that "SediGraph 5100 particle size measurements indicate KGa-IB is 57.8% <2 *μm* and 32.0% <0.5 *μm* whereas KGa-1 is 47.3% <2 *μm* and 21.4% <0.5 *μm*.". Żbik and Smart summarize the general description of KGa-1 as "Ninety percent by weight of the particles have an equivalent spherical diameter less than *2 μm* with a median particle size of 0.7 μm and specific surface area of 15.3 ± 0.5 *m²/gr* (BET nitrogen adsorption)". Pruett and Webb report BET surface area measurements of 8.4 and 11.7 m²/gr for KGa-1 and KGa-1B respectively. Reported ranges of aspect ratios for KGa-1 from Brady *et al.* (1996) and Żbik and Smart (1998) are 2 to 10 and 4 to 8 respectively. The median particle size of 0.7 μm described by Żbik and Smart fall well within the measured particle sizes.

For validation purposes two scenarios are considered. In the first scenario, the known general morphology of the particles will be used to assess the validity of the portrayed dynamics and flow model. In the second scenario it is assumed that there is no knowledge of the geometry in order to find what is there to reveal about the morphology from the settling velocity.

Assuming a standard temperature of *15* Cᵒ the measured settling velocity for the size defining 50 % finer by Lu et al. (Stokes' radius ≈ 0.275 *μm*) of Georgia kaolinite is in the order of 2.7×10⁻⁷ *m/s*. If we assume knowledge of the aspect ratio only in the order of 10 in Eq. (60), the oblate spheroid has dimensions *2a = 1.86 μm* and *2b = 0.186 μm*. Note the close agreement with the SEM analysis. Considering an aspect ratio of 9 for KGa-1 median particle reported by

Żbik and Smart (0.7 *μm* equivalent diameter) is an oblate spheroid of dimensions *2a = 2.26 μm* and *2b = 0.25 μm*. Using coin like structures for the mica particles and a thickness of *6.7 μm* Eq. (60) satisfies for the mean particle velocity of *5.7 ×10⁻⁴ m/s*. Variation of the thickness from *2* to *8 μm* satisfy for the entire range of experimental values.

For the second scenario note also that a thickness for the large aspect ratio particle and an equivalent diameter can also be easily computed for any velocity. Equation (60) turns into the settling velocity of spheres as portrayed by Eq. (34) for either coins or the oblate spheroid model when the aspect ratio is 1. As there is always an equivalent sphere for a flat particle one can write:

$$\frac{4b^2 e_{max}^2}{9(1+f(a,b))^2} \frac{(0.0001+\xi_{1max})}{(0.0001+h_{e1max}^2)} = r_s^2 \xi_{max} \qquad (61)$$

hence,

$$b = \frac{3r_s \xi_{max}^{1/2}}{2e_{max}} \frac{(1+f(a,b))(0.0001+h_{e1max}^2)^{1/2}}{(0.0001+\xi_{1max})^{1/2}} \qquad (62)$$

The fraction on the right depends only on the aspect ratio for the given temperature and fluid. Note the role of the expansion and the tributary ratio to account for different densities of solids and fluid. Let us return to the experimental results to note that the 0.7 and 0.5 *μm* size particles of kaolinite (*Gs* = 2.62) described at assumed temperature of *15° C* settled at approximately 0.380 and 0.194 *μm/s* respectively. By means of Eq. (62) the simple graph shown in Fig. 2 defines the general geometry of all the oblate spheroids and coins settling at the given velocities.
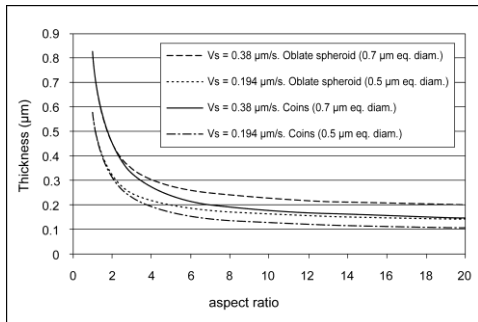

Fig. 2. Combination of aspect ratio thickness of particles with Gs = 2.62 settling at 0.380 and 0.194 *μm/s* for coins and oblate spheroids.

Based on TEM micrographs Żbik *et al.* (2007) describes the course fraction of KGa-1 as "pseudo-hexagonal in shape plates a few micrometers in size". Żbik and Frost (2009) show an SEM image showing the finest colloidal fraction of KGa-1. The clay particles are pseudo hexagonal euhedral crystals of approximately 0.75 μm in major dimension with a few exceptions in the range of 0.14 to 0.35 *μm*. Żbik and Frost inferred an average aspect ratio of 5.3. Note also that the range of particle sizes for "as shipped" KGa-1 may range in the order of 0.1 to 40 μm (Chipera and Bish 2001) in equivalent diameter and the sample may contain "larger

stacks and defoliated pseudo-hexagonal in shape plates a few micrometers in size" Żbik *et al.* (2007). Using the ranges of aspect ratio given in the literature, Eq. (62), as noted in Fig. 2 is in good agreement with the observed morphology. Given that the velocity profile is modeled along the flatter side of the particle the good agreement also suggests that, as expected, the particles settle along its long axis. Equation (62) embraces the discussion regarding the influence of particle size and shape in settling phenomena to furnish great advantage in sedimentation analysis. It also adds practical significance to the research effort in morphology and specific surface area of clay particles.

9. CONCLUSION

From the beginning of the study of the principles of fluid dynamics the impact of the kinetic energy, pressure drags and the viscosity concepts has been naturally linked to the forces mobilized by fluids against solid objects or vice versa. For large particles or objects logical and experimental evidence show that the motion occurs by displacement of fluid by the kinetic energy and in a smaller quantity by viscous shear. It is a natural approach to use the same logic for creeping motion. However, this paper suggests and substantiates that in creeping motion the displacement of fluid occurs by shear rates only, i.e. the shear resistance of the fluid is comparable with the shear stress mobilized by the particle. The equilibrium condition is satisfied by the transfer of the force to the fluid medium in the form of a pressure gradient and the magnitude of the pressure gradient is the result of the contest of the body forces against the shear forces. Not only the flow model derived in this paper provides useful insights of the fluid dynamics in creeping motion but also provided a rational approach to derive a flow model for non spherical particles in creeping motion. The model shows that settlement analysis of natural occurring materials can be performed with very basic knowledge of their morphology and embrace the influence of particle size and shape in sedimentation phenomena.

REFERENCES

Al-Naafa, M.A. and M.S. Selim (1992). Sedimentation of monodisperse and bidisperse hard-sphere colloidal suspensions. *AIChE Journal, American Institute of Chemical Engineers* 38(10), 1618-1630.

Arkangel'skii, B.V. (1935). Experimental Study of Accuracy of Hydraulic Coarseness scale of Particles. *Isv. NHG* 15, Moscow, Russia (in Russian).

Bickmore, B.R., K.L. Nagy, P.E. Sandlin and T.S. Crater (2002). Quantifying surface areas of clays by atomic force microscopy. *American Mineralogist* 87, 780-783.

Blum, A.E. and D.D. Eberl (2004). Measurement of clay surface areas by polyvinylpyrrolidone (pvp) sorption and its use for quantifying illite and smectite abundance. *Clays and Clay Minerals* 52(5), 589-602.

Brady, P., R. Cygan and K. Nagy (1996). Molecular Controls on Kaolinite Surface Charge. *Journal of Colloid Interface Science* 183(2), 356-364.

Cadene A., S. Durand-Vidal, S. Turq and J. Brendle (2005). Study of individual Na-montmorillonite particles size, morphology, and apparent charge. *Journal of Colloid and Interface Science* 285(2), 719-730.

Cheng, N. (1997). Simplified Settling Velocity Formula for Sediment Particle. *Journal of Hydraulic Engineering* 123(2), 149-152.

Chipera, S. and D. Bish (2001). Baseline Studies of the Clay Minerals Society Source Clays: Powder X-Ray Diffraction Analyses. *Clays and Clay Minerals* 49(5), 398-409.

Gibson, W.H. and L.M. Jacobs (1920). The Falling Sphere Viscosimeter. *Journal of the Chemical Society, Transactions* 117, 473-478.

Goodstein, D. (2000). In the Case of Robert Andrews Millikan. *Engineering and Science* 4, 30-38.

Inoue, A. and R. Kitagawa (1994). Morphological characteristics of illite clay minerals from hydrotermal system. *American Mineralogist* 79, 700-711.

Jinghwa Hsü, K. (2004). *Physics of Sedimentology.* 2nd ed., Germany, Springer.

Jodin, M.C., F. Gaboriaud and B. Humbert (2004). Repercussions of size heterogeneity on the measurement of specific surface areas of colloidal minerals: Combination of macroscopic and microscopic analyses. *American Mineralogis* 89, 1456.

Lu, N., G. Ristow and W. Likos (2000). The accuracy of hydrometer analysis for fine-grained clay particles. *Geotechnical Testing Journal* 33(4), 487-495.

Millikan, R.A. (1913). On the elementary electric charge and the Avogadro constant. *Physical Review* 2(2), 109-143.

Nadeau, P.H. (1987). Relationships between the mean area, volume and thickness for dispersed particles of kaolinites and micaceous clays and their application to surface area and ion exchange properties. *Clay Minerals* 22(3), 351-356.

Nadeau, P.H. (1985). The physical dimensions of fundamental clay particles. *Clay Minerals* 20, 499-514.

Pruett, R. and H. Webb (1993). Sampling and analysis of KGa-1 B well-crystallized kaolin source clay. *Clays and Clay Minerals* 41(4), 514-519.

Santamarina, J.C., K.A. Klein, Y.H. Wang and E. Prencke (2002). Specific surface: determination and relevance. *Canadian Geotechnical Journal* 39, 233-241.

Sarkisyan, A.A. (1958). *Deposition of Sediment in a Turbulent Stream.* Izd. AN SSSR, Moscow, Russia (in Russian).

Sayed Hassan, M., F. Villieras, F. Gaboriaud and A. Razafitianamaharavo (2006). AFM and low-pressure argon adsorption analysis of geometrical properties of phyllosilicates. *Journal of Colloid and Interface Science* 296, 614-623.

Van Olphen, H., and J.J. Fripiat (1979). *Data handbook for clay materials and other non-metallic minerals.* Oxford, England, Pergamon Press.

White, F.M. (1994). *Fluid Mechanics.* 3rd ed., New York, McGraw-Hill, Inc.

Yukselen, Y. and A. Kaya (2006). Comparison of methods for determining specific surface area of soils. *Journal of Geotechnical and Geoenvironmental Engineering* 132(7).

Żbik, M. and R. Frost (2009). Micro-structure differences in kaolinite suspensions. *Journal of Colloid and Interface Science* 339(1), 110-116.

Żbik, M., R. Frost, Y. Song, Y. Chen and J. Chen (2007), Transmission x-ray microscopy reveals the clay aggregate discrete structure in aqueous environment. *Journal of Colloid Interface Science* 319(2), 457-461.

Żbik, M. and R.St. Smart (1998). Nanomorphology of kaolinites: comparative SEM and AFM studies. *Clays and clay Minerals* 46(2), 152-160.

Zegznda, A.P. (1934). Settlement of sand gravel particles in still water. fev. NIIG 12, Moscow, Russia (in Russian).

Zhu, L.J. and N.S. Cheng (1993). *Settlement of Sediment Particles.* Research Report, Department of River and Harbor Engineering, Nanjing Hydraulic Research Institute, Nanjing, China (in Chinese).